



## Article

# Flow Control of Radial Inlet Chamber and Downstream Effects on a Centrifugal Compressor Stage

Fenghui Han <sup>1,2</sup> , Zhe Wang <sup>1,\*</sup> , Yijun Mao <sup>3</sup>, Jiajian Tan <sup>4</sup> and Wenhua Li <sup>1,2</sup>

<sup>1</sup> Marine Engineering College, Dalian Maritime University, Dalian 116026, China; fh.han@dmlu.edu.cn (F.H.); lwh992@dmlu.edu.cn (W.L.)

<sup>2</sup> National Center for International Research of Subsea Engineering Technology and Equipment, Dalian Maritime University, Dalian 116026, China

<sup>3</sup> School of Aerospace Engineering, Huazhong University of Science & Technology, Wuhan 430074, China; maoyijun@hust.edu.cn

<sup>4</sup> Department of Research & Development, Shenyang Blower Works Group Co., Ltd., Shenyang 110869, China; tanjiajian@shengyu.com.cn

\* Correspondence: zhe.wang.work@gmail.com; Tel.: +86-0411-84729038

**Abstract:** Radial inlet chambers are widely used in various multistage centrifugal compressors, although they induce extra flow loss and inlet distortions. In this paper, the detailed flow characteristics inside the radial inlet chamber of an industrial centrifugal compressor have been numerically investigated for flow control and performance improvement. First, the numerical results are validated against the experimental data, and flow conditions inside the inlet chambers with different structures are compared. They indicate that, in the non-guide vane scheme, sudden expansions, tangential flows and flow separations in the spiral and annular convergent channels are the major causes of flow loss and distortions, while using guide vanes could introduce additional flow impacts, separations and wakes. Based on the flow analysis, structure improvements have been carried out on the radial inlet chamber, and an average increase of 4.97% has been achieved in the inlet chamber efficiencies over different operating conditions. However, the results further reveal that the increases in the performance and overall flow uniformity just in the radial inlet chamber do not necessarily mean a performance improvement in the downstream components, and the distribution of the positive tangential velocity at the impeller inlet might be a more essential factor for the efficiency of the whole compressor.



**Citation:** Han, F.; Wang, Z.; Mao, Y.; Tan, J.; Li, W. Flow Control of Radial Inlet Chamber and Downstream Effects on a Centrifugal Compressor Stage. *Appl. Sci.* **2021**, *11*, 2168. <https://doi.org/10.3390/app11052168>

Academic Editors: Minsuk Choi and Maria Grazia De Giorgi

Received: 28 January 2021

Accepted: 24 February 2021

Published: 1 March 2021

**Publisher's Note:** MDPI stays neutral with regard to jurisdictional claims in published maps and institutional affiliations.



**Copyright:** © 2021 by the authors. Licensee MDPI, Basel, Switzerland. This article is an open access article distributed under the terms and conditions of the Creative Commons Attribution (CC BY) license (<https://creativecommons.org/licenses/by/4.0/>).

**Keywords:** centrifugal compressor; radial inlet chamber; guide vanes; flow control; performance improvement; downstream effect

## 1. Introduction

Centrifugal compressors, as important general purpose equipment, are widely used in the aerospace, chemical, power and energy industries, but they are also highly energy-consuming machinery in industrial systems [1,2]. The devices that transport working fluids from the pipelines or the atmosphere to the impeller inlet are called inlet chambers, and radial inlet chambers are the key upstream component widely used in large-scale multistage centrifugal compressors due to the layout constraints of compact industrial systems [3,4]. However, compared with axial inlet ducts, the radial inlet chamber will introduce extra flow loss and distortions, which negatively influence the compressor's performance [5,6]. Therefore, it requires an improved design to avoid flow separations in the chamber, reduce flow loss and achieve uniform flow distribution at the outlet of the radial inlet chamber [7,8].

There are a lot of studies that have been carried out on the impacts of upstream components, including the intake ducts [9], upstream bends [10] and guide vanes [11]. Galindo et al. [12,13] experimentally measured the steady compressor map from a turbocharger and studied the effect of a swirl generator device on the surge margin of the

turbocharger compressor with a radial inlet bend. The results indicated that the surge limits were improved when the flow pre-whirl was opposite to the rotational direction of the impeller. MacManus et al. [14] and Yamada et al. [15] conducted research on the S-duct and 90 degree bent pipes in the upstream of single-stage centrifugal compressors and investigated the influences of corresponding swirling distortions on the impeller and diffuser, respectively. Zhang et al. [16] further analyzed the effect of inlet tortional pipes with two elbows on the performance and pressure distribution of the compressor with a volute. However, compared with these upstream curved pipes used in single-stage centrifugal compressors for turbochargers, the radial inlet chambers used in large-scale multistage centrifugal compressors for industrial systems have a more complex structure with more complicated flow distortions, and the flow loss is more significant. In general, using a radial inlet chamber will lead to a decrease of 2–4% in the performance of the compressor stage while the corresponding design and optimization methods still stay, in theory [17,18].

As the basis for the improvement research, the flow characteristics inside the radial inlet chambers were analyzed. Flow measurements were carried out by Flathers et al. [19] at the outlet of the inlet chamber from an industrial centrifugal compressor, which experimentally proved the flow loss and distortions generated in the chamber. With the aid of the computational fluid dynamics (CFD) method, Koch et al. [20] found that the flow loss in the inlet chamber was positively related to the inlet Mach number, but the flow characteristics inside the chamber almost remained unchanged under different Mach numbers. Michelassi et al. [21] and Pazzi et al. [22] used a combination of experiments and numerical simulations to study the scale models of radial inlet chambers without the influence of downstream impellers, and the distributions of the velocity magnitude, flow angle and loss coefficient at the outlet of the inlet chamber were obtained and analyzed. Han et al. [23,24] conducted a large-scale flow measurement on the main sections in a radial inlet chamber, including the inlet and outlet of the chamber, the intake channel's outlet and the spiral channel's outlet. The measurement was composed of more than 900 testing points on the four cross-sections, and the detailed distributions of the flow parameters inside the radial inlet chamber were first published in the open literature.

Then, studies on the improvement of the radial inlet chambers were performed. Kim et al. [25] arranged a converging structure and adopted two rows of guide vanes to improve the flow condition at the outlet of the inlet chamber. An indicator function related to the geometric parameters was developed by Saladino et al. [26] and used to minimize the flow loss of the radial inlet chamber. Yagi et al. [27] obtained the distribution of the flow loss in the inlet chamber and the distortions of its outlet flow, based on which the cross-sectional area was selected as the key parameter for structure optimization. Kozhukhov et al. [28] compared the local loss coefficient at the exits of different inlet chambers and analyzed the main geometric parameters related to the flow loss. Sezal et al. [29] found that the circumferentially nonuniform variable inlet guide vanes in the radial inlet chamber were more adaptable to the incoming flow angle, which could reduce the flow loss by 40%. In addition to the optimization of the radial inlet chamber itself, its impact on the downstream components is also a key issue to the performance of the entire compressor. Tan et al. [30] studied the effects of radial inlet chambers on the performance of a centrifugal compressor stage with inlet guide vanes. The results indicated that, compared with the uniform axial intake, the efficiency and total pressure ratio of the compressor stage with a radial inlet chamber decreased by an average of 2.5% and 1%, respectively, over the entire operating range, and the regulation performance of the inlet guide vanes was also adversely affected. Han et al. [31] carried out experimental and numerical studies on the radial inlet stages of two different industrial centrifugal compressors and analyzed the effects of the internal flow loss and the outlet distortion of the inlet chambers on the performance of the downstream components.

According to the literature review, it was found that flow loss and distortions were the two main factors that affected the performances of the inlet chamber itself and the

downstream components in the compressor. However, the influence mechanism of the radial inlet chamber on the entire centrifugal compressor has still not been completely revealed, and the following problems remain unsolved. First, in the previous research, the optimization objects of the radial inlet chambers were either to reduce the flow loss or increase the uniformity of the outlet flow without considering these two factors together. This approach has limited a more comprehensive improvement of the radial inlet chamber. Second, although it is known that the flow uniformity at the impeller inlet is essential for the compressor stage, the complex flow distortions induced by the radial inlet chamber involve many parameters (e.g., the uneven distributions of pressures, velocity magnitudes and distortions of different velocity components), and which is the most important to the performance of the entire compressor is still unknown. This hinders further improvement in the performances of centrifugal compressors with radial inlet chambers. Meanwhile, the inlet guide vanes analyzed in the previous studies are generally arranged downstream or without the inlet chamber, while there is less research related to the guide vanes inside the radial inlet chambers.

With the development of numerical theory and computational technology, CFD methods are widely used for flow analysis and structure improvement in various engineering applications [32–34]. Therefore, in this paper, numerical simulations are performed on the radial inlet chamber with and without guide vanes to figure out the mechanism of flow loss and distortions generated in the inlet chamber. Then, in order to solve the first problem, the flow loss and distortions are considered together to obtain an improved design of the radial inlet chamber. Finally, for the second problem, the major parameters related to the flow uniformity are investigated at the impeller inlet, expecting to develop an in-depth understanding of the influence mechanism and provide guidance for further improvement of centrifugal compressors with radial inlet chambers.

## 2. Methodology

### 2.1. Flow Configuration

The research object of this paper is the radial inlet chamber coming from the inlet stage of a multistage centrifugal compressor, which is an industrial product of SBW (Shenyang Blower Works Group Co., Ltd., Shenyang, China). The working fluid of the compressor is air, and its mass flow rate at the design condition is 4.29 kg/s. Figure 1 shows the schematic diagram of the radial inlet chamber (from *in* to 0) and the first stage of the centrifugal compressor (from 0 to *out*). As a typical structure for a radial inlet, this chamber mainly consists of an intake channel, a spiral channel and an annular convergent channel, where  $b_e$  and  $r_c$  are the width and radius of the spiral channel, respectively,  $w_e$  is the intersecting width of the intake channel and the spiral channel and  $b_I$  is the inlet width of the annular convergent channel. The major geometric parameters of the original radial inlet chamber and the first stage of the compressor are listed in Table 1.

**Table 1.** Major geometric parameters of the radial inlet chamber and the compressor stage.

Radial Inlet Chamber	Size	Compressor Stage	Size
Inlet diameter $D_{in}$	460 mm	Inlet diameter of impeller $D_0$	298 mm
Intersecting width $w_e$	590 mm	Outlet diameter of impeller $D_2$	400 mm
Width of spiral channel $b_e$	220 mm	Outlet width of impeller $b_2$	40 mm
Radius of spiral channel $r_c$	480 mm	Number of impeller blades $Z$	17
Inlet width of annular channel $b_I$	110 mm	Outlet diameter of diffuser $D_4$	641 mm
Inlet diameter of annular channel $D_I$	440 mm	Outlet width of diffuse $b_4$	37.3 mm

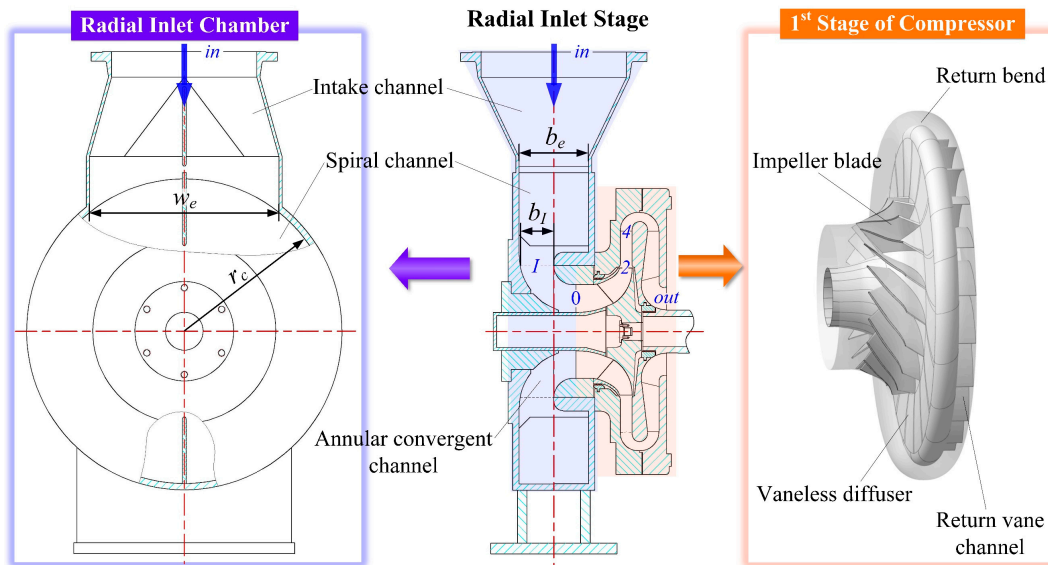


Figure 1. Schematic diagram of the radial inlet chamber and the compressor stage.

## 2.2. Numerical Method

### 2.2.1. CFD Code

The governing equations used to model the internal flow of the radial inlet chamber and the centrifugal compressor are the three-dimensional steady and compressible Reynolds-averaged Navier–Stokes equations. The general expression of the governing equations in a Cartesian frame can be written as

$$\frac{\partial}{\partial t} \int_{\Omega} U d\Omega + \int_S \vec{F}_I \cdot d\vec{S} + \int_S \vec{F}_V \cdot d\vec{S} = \int_{\Omega} S_T d\Omega \quad (1)$$

where  $\Omega$  and  $S$  represent the volume and the surface, respectively,  $U$  is the vector of the conservative variables and  $\vec{F}_I$  and  $\vec{F}_V$  are the inviscid and viscous flux vectors, respectively. Assuming that the flow inside the centrifugal compressor is adiabatic, the source term vector  $S_T$  contains the contributions of the Coriolis and centrifugal forces, which is expressed as [30]

$$S_T = \begin{bmatrix} 0 \\ (-\bar{\rho}) \left[ 2\vec{\omega} \times \vec{w} + (\vec{\omega} \times (\vec{\omega} \times \vec{r})) \right] \\ \bar{\rho} \vec{w} \cdot \vec{\nabla} (0.5\omega^2 r^2) \end{bmatrix} \quad (2)$$

The flow solver EURANUS [35] of the commercial software NUMECA FINE/Turbo, Brussels, Belgium was employed for the numerical simulations in the present study; it performs a finite volume scheme for the spatial discretization and adopts a multistage Runge–Kutta scheme for the temporal discretization. In addition, a multi-grid strategy, local time stepping and implicit residual smoothing technology were applied in the CFD code to accelerate the calculation convergence. In order to make the equation system closed, it was necessary to adopt the corresponding fluid model and choose a proper turbulence model to specify the relationship between the pulsation value and the time-averaged value of the turbulent flow. In this paper, the working fluid was air, which was treated as a perfect gas. The Spalart–Allmaras model was chosen for the turbulence closure, which has been proven to ensure sufficient accuracy in predicting the flow conditions inside compressors with radial inlet chambers [30,31].



### 2.2.2. Computational Models

In order to investigate the flow characteristics inside the radial inlet chamber and its effects on the first stage of the compressor in the downstream, two sets of computational models were employed in the present study. For the flow analysis of the inlet chamber itself, the computational model included a radial inlet chamber (with or without guide vanes), a straight inlet pipe and an outlet pipe, as shown in Figure 2a. All the patches were modeled with data from the previous experimental research [36,37]. Meanwhile, as shown in Figure 2b, a computational model of the radial inlet compressor stage was built for the study on the performance improvement and downstream effects of the radial inlet chamber.

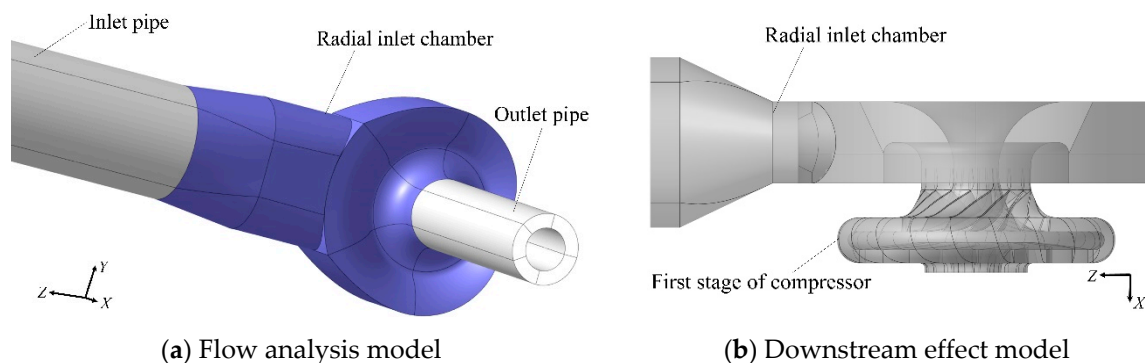


**Figure 2.** Computational models for flow analysis and the downstream effects of the radial inlet chamber.

The boundary conditions for the CFD models were imposed according to the actual operating data. For the flow analysis model, the uniformly distributed total pressure and total temperature were adopted as the inlet boundary conditions at the entrance of the inlet pipe with a flow direction along the pipe axis, and the mass flow rate as the outlet boundary condition was set at the end of the outlet pipe using the velocity scaling method. For the downstream effect model, specific profiles extracted from the fully developed flow were provided at the entrance of the radial inlet chamber (i.e., *in* in Figure 1), and the mass flow rate was imposed at the outlet of the first compressor stage (i.e., *out* in Figure 1). All the solid walls were set as adiabatic and non-slip boundaries with hydraulically smooth surfaces.

In order to achieve the final convergent solutions for the flow analysis, both the residual convergence and the mass flow convergence were taken into consideration. When the global residuals stayed lower than  $10^{-6}$  and the deviation between the inlet and outlet mass flow rates was less than 0.5%, the numerical solutions were considered to be converged.

## 2.3. Verification and Validation

### 2.3.1. Grid Convergence Study

Structured multi-block grids were generated for all the components using NUMECA IGG, and particular attention was paid to the grid refinements close to the solid walls. A grid convergence study was performed for all the CFD models to verify the grid independence of the numerical results in the present research. Here, the flow analysis model of the radial inlet chamber with eight guide vanes was provided as an instance for the comparison of the numerical results obtained with different grid resolutions. In order to verify grid independence, seven groups of computational grids were generated for this numerical model, and the changes in grid elements in each component followed the grid convergence method (GCI) provided by ASME (American Society of Mechanical Engineers) [38,39]. Detailed grid distributions of the computational components in different schemes are listed in Table 2.

**Table 2.** Verification schemes for the convergence study.

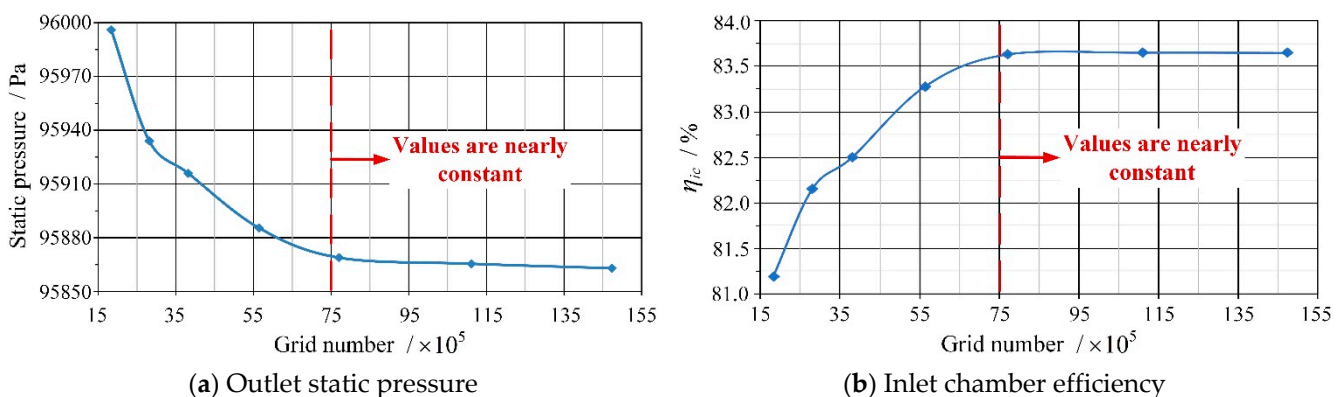
No.	Inlet Pipe	Radial Inlet Chamber	Guide Vanes	Outlet Pipe	Total Grid Number
1	$1.4 \times 10^5$	$5.8 \times 10^5$	$6.0 \times 10^5$	$5.1 \times 10^5$	$1.8 \times 10^6$
2	$2.2 \times 10^5$	$8.9 \times 10^5$	$9.0 \times 10^5$	$8.1 \times 10^5$	$2.8 \times 10^6$
3	$3.1 \times 10^5$	$1.2 \times 10^6$	$1.2 \times 10^6$	$1.1 \times 10^6$	$3.8 \times 10^6$
4	$4.5 \times 10^5$	$1.8 \times 10^6$	$1.7 \times 10^6$	$1.6 \times 10^6$	$5.6 \times 10^6$
5	$6.2 \times 10^5$	$2.5 \times 10^6$	$2.4 \times 10^6$	$2.2 \times 10^6$	$7.7 \times 10^6$
6	$9.1 \times 10^5$	$3.5 \times 10^6$	$3.4 \times 10^6$	$3.3 \times 10^6$	$1.1 \times 10^7$
7	$1.2 \times 10^6$	$4.7 \times 10^6$	$4.6 \times 10^6$	$4.3 \times 10^6$	$1.5 \times 10^7$

As the grid number changed, the variations of the major flow parameters (e.g., the pressure, temperature and velocity) on the main sections were monitored and compared. The performance parameters were also analyzed for the CFD model. As a stationary component, the flow efficiency  $\eta_{ic}$  and total pressure loss coefficient  $\zeta_{ic}$  of the radial inlet chamber are expressed as

$$\eta_{ic} = \frac{\kappa}{\kappa - 1} \cdot \frac{\ln(T_{s,0}/T_{s,in})}{\ln(p_{s,0}/p_{s,in})} \quad (3)$$

$$\zeta_{ic} = (p_{t,in} - p_{t,0}) / \left( \frac{1}{2} \rho_{in} V_{in}^2 \right) \quad (4)$$

Figure 3 shows the trends of the outlet static pressure and inlet chamber efficiency under the seven grid resolutions, where the flow parameters were extracted from the mass-averaged values in the corresponding sections. It can be clearly seen that when the grid number was less than a certain limit (e.g.,  $7.5 \times 10^6$  for this particular case), both the static pressure at the model's exit and the efficiency of the radial inlet chamber significantly changed with the variation of the grid number. However, when the number of grids increased to Mesh 5 =  $7.7 \times 10^6$  elements, the flow and performance parameters almost remained unchanged, and the maximum deviations of the static pressures and efficiencies obtained by Mesh 5, Mesh 6 and Mesh 7 were only 0.006% and 0.019%, respectively. The results of the other flow parameters also indicate that, when the grid elements increased to the number marked with a red line in the figure, there was little difference in the numerical results obtained with different grid resolutions. Therefore, Mesh 5 was considered to ensure sufficient accuracy for the numerical simulation of this radial inlet model. For the first stage of the compressor downstream from the radial inlet chamber, the grid convergence study also proved that the probable uncertainties caused by the computational grids were less than 0.03% [31]. The final computational grids for different components of the CFD models are shown in Figure 4.

**Figure 3.** Variations of the flow and performance parameters with the grid number.

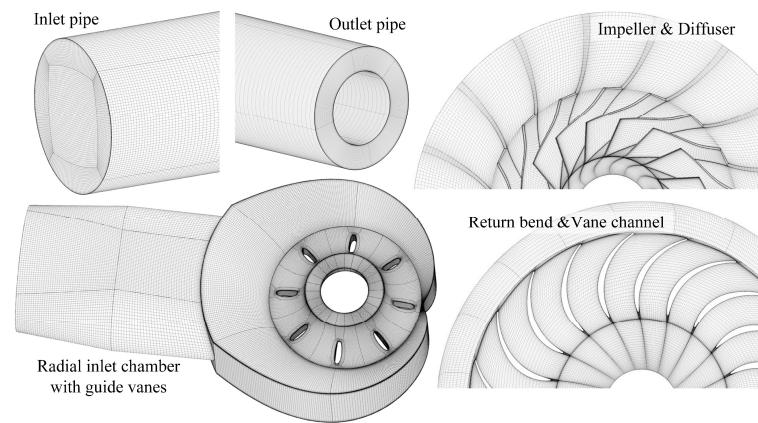


**Figure 4.** Computational grids for different components of the computational fluid dynamics (CFD) models.

Considering that different turbulence models have specific requirements for the distance from the first node of the grid to the solid wall, the  $y^+$  values obtained with the above computational grids were checked in Figure 5. It can be found that the  $y^+$  values of over 90% for the solid surfaces were in the range of 1–8, and the maximum  $y^+$  value was less than 10, which met the requirement of the Spalart–Allmaras turbulence model employed in this paper. In addition, the qualities of the computational grids are provided in Table 3, proving that good grid quality was achieved for the present numerical solutions.

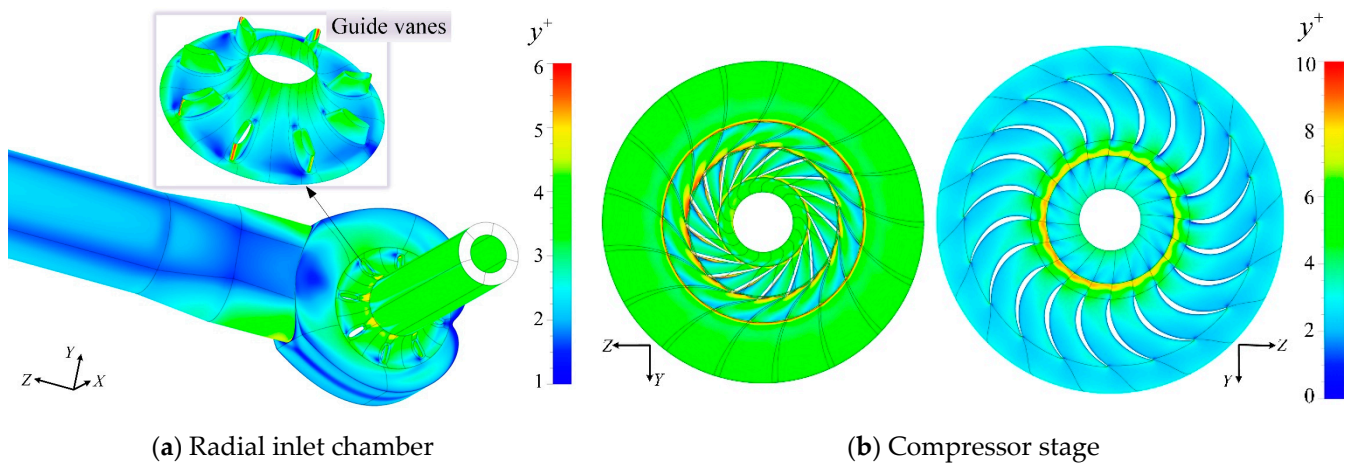


**Figure 5.**  $y^+$  distributions of the computational grids.

**Table 3.** Grid quality of the computational models.

Item	Radial Inlet Chamber	Guide Vanes	Compressor Stage	Recommended Value [40,41]
Minimum orthogonality	34.3°	33.2°	21.3°	>10°
Maximum aspect ratio	750	408.9	839	<5000
Maximum expansion ratio	1.51	1.91	3.84	<5

### 2.3.2. Validation of the Numerical Method

In order to validate the reliability of the numerical results in the present study, the calculated flow parameters on the main sections in the radial inlet chamber and the predicted performance of the compressor stage were extracted and compared against the experimental results of the previously published literature [36,37].

Figure 6 shows the detailed flow distributions for the inlet and internal sections of the radial inlet chamber in the form of dimensionless Mach numbers. Compared with

the experimental data, the ranges of the mainstreams for the sections were larger in the numerical results with a higher velocity gradient close to the wall, which was mainly caused by the smooth wall assumption of the CFD model. Since the machining chamfers and fillets were simplified in the numerical models to facilitate the grid meshing, small deviations would also be introduced to the flow simulation. Except for these slight differences, the flow characteristics predicted by the numerical method agreed well with the experimental data. This revealed that the CFD results obtained in this paper performed well in capturing the major characteristics and key details of the flow conditions inside the radial inlet chambers, which ensured an acceptable accuracy for the numerical flow analysis.

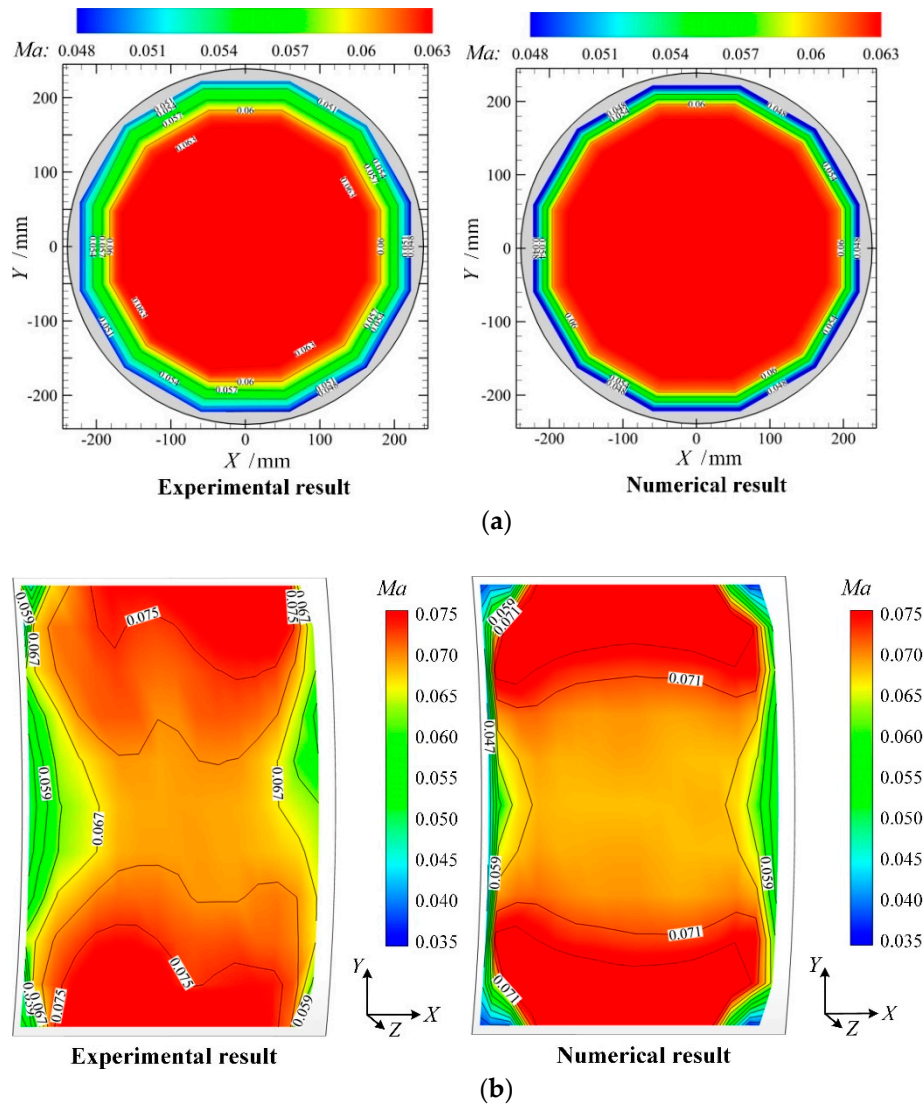


**Figure 6.** Comparison of the measured and simulated Mach numbers in the radial inlet chamber. (a) Results for the inlet section. (b) Results for the interface of the intake and spiral channels.

For the CFD results of the compressor stage, a performance comparison between the numerical simulation and the model test was made under different operating conditions at the design’s rotational speed. The predicted and measured performance parameters of the compressor stage (from 0 to out) are shown in Figure 7. The mass flow was dimensionless by the design’s flow rate, and the total pressure ratio  $\epsilon$  and polytropic efficiency  $\eta$  are calculated as follows [42]:

$$\epsilon_{0-out} = p_{t,out} / p_{t,0} \tag{5}$$



$$\eta_{0-out} = \frac{\kappa}{\kappa - 1} \cdot \frac{\ln(p_{t,out}/p_{t,0})}{\ln(T_{t,out}/T_{t,0})} \quad (6)$$

It can be clearly seen that the trend of the compressor performance curves obtained by the numerical simulation agreed well with the experimental data. For the whole compressor stage, the differences between the numerical and experimental results were less than 3% under most of the operating conditions. This further validates the reliability of the numerical method and computational results in the present research.

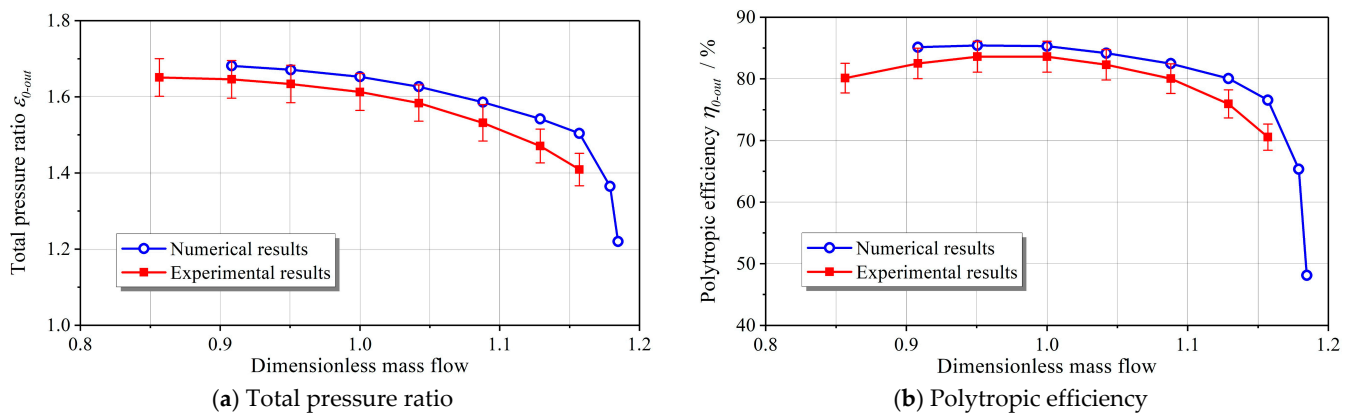


Figure 7. Comparison of the numerical and experimental performances for the compressor stage.

### 3. Flow Analysis

The flow characteristics inside the radial inlet chamber were analyzed at the design conditions. The exit of the radial inlet chamber (i.e., 0 in Figure 1) was a key section analyzed in this paper, since the flow condition here is an important factor affecting the performance of the downstream components. Figure 8 shows the flow distributions of this section of the radial inlet chambers with and without guide vanes, including the Mach numbers, velocity vectors and total pressure contours. This revealed that a pair of vortices opposite to each other were captured on the left side of this section, and the distributions of the Mach numbers and total pressure in the two schemes had the same trends from the left to the right.

The numerical results of the scheme without guide vanes in Figure 8a reveal a low-pressure and low-speed separation area on the side, close to the intake channel of the radial inlet chamber. When the guide vanes were arranged in the annular convergent channel, this flow separation disappeared, as shown in in Figure 8b, and instead, two vortices of a larger size were clearly observed in this area. This was mainly because when the high-speed airflow from the intake channel turned 90° in the axial direction, it impacted the guide vanes and slowed down, which greatly weakened the flow separation caused by the 90 degree turning. Meanwhile, the flow impacting on the leading edges of the guide vanes induced extra separations and wake flows, resulting in more obvious vortices downstream of the 90 degree turning at the exit.

The three-dimensional streamlines of the radial inlet chambers are shown in Figure 9. It can be found that, when the impeller was absent, the flow field was symmetric with respect to the X-Z plane. According to the streamlines, the fully developed incoming flow from the intake channel entered the spiral channel and was divided into different paths. Part of the airflow kept the direction almost unchanged and flowed into the annular convergent channel along the shortest path, while the rest of the fluid expanded at the spiral channel inlet and generated two pairs of sudden expansion vortices on both sides, which continued to develop toward the downstream. When the airflow turned 90° to the convergent channel, flow separations were easier to form at the inner radius due to the large curvature. As the fluid flowed along the tangential direction in the spiral channel, it was guided by the convergent structure of the bottom walls in the radial inlet chamber



and was gradually redirected into the annular convergent channel without generating more separations. It can be found that the flow separations and vortices were mainly formed in the spiral channel and the convergent channel, which were the major causes of the flow loss in the radial inlet chambers.

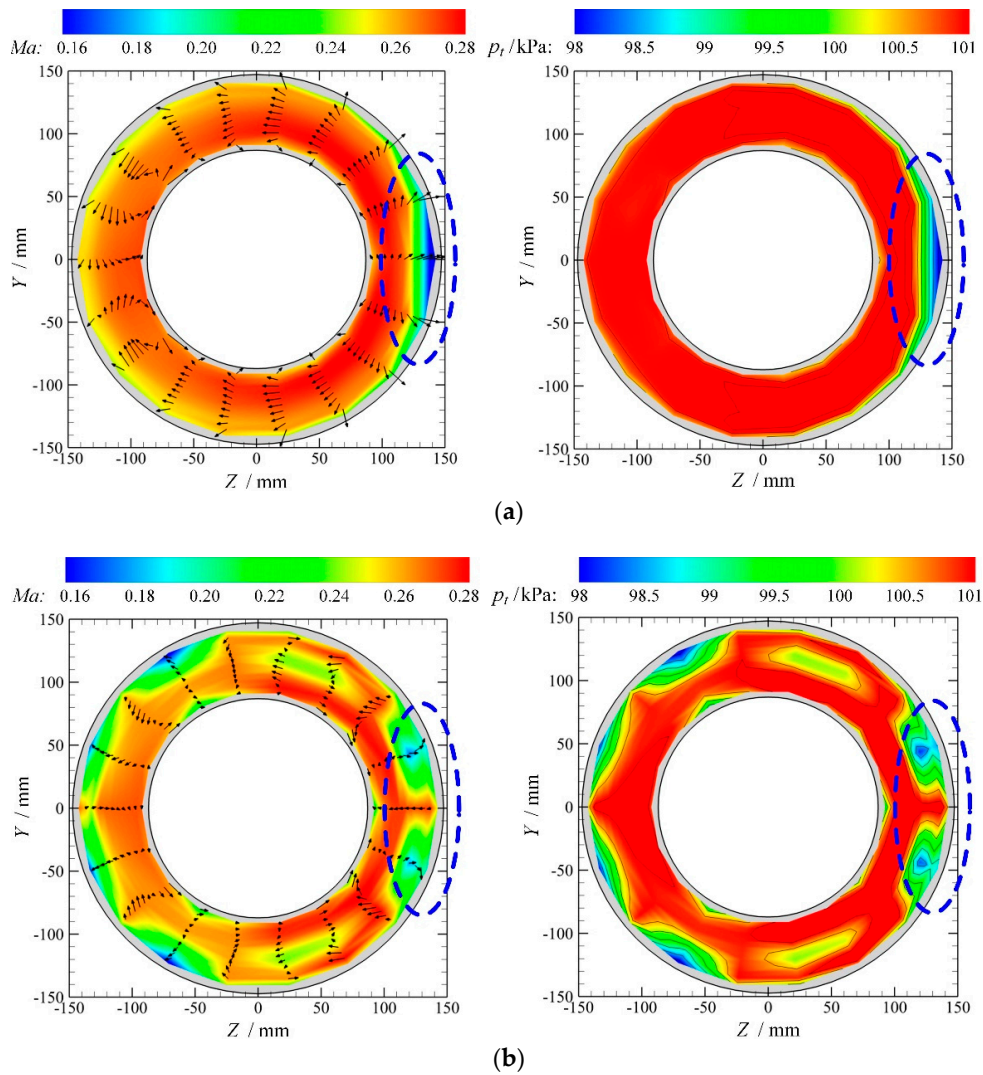
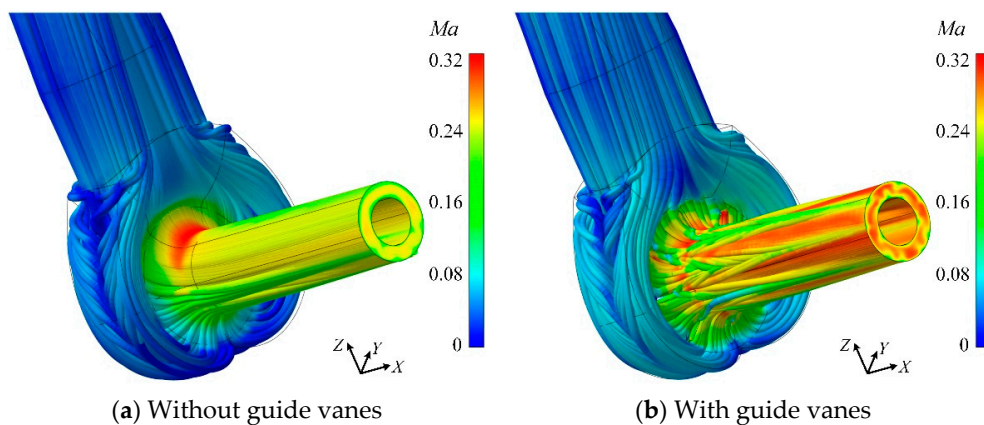


Figure 8. Flow distributions at the exit of the radial inlet chamber (a) without guide vanes and (b) with guide vanes.



(a) Without guide vanes (b) With guide vanes

Figure 9. Three-dimensional streamlines inside the radial inlet chambers.

In order to further analyze the flow mechanism, detailed distributions of the vorticity and entropy in the middle section of the spiral and annular convergent channels are provided in Figure 10. In the inlet chamber without guide vanes, it was observed that the entropy productions mainly occurred on both sides of the spiral channel and the 90 degree turning of the convergent channel where a high vorticity magnitude appeared, while the entropy was quite low on the upper side close to the intake channel due to the low vorticity magnitude in this area. This resulted in uneven flow distributions along the circumferential direction, which would deteriorate the flow condition in the downstream compressor. Therefore, guide vanes were employed to reduce the unevenness at the exit of the radial inlet chamber. However, as shown in Figure 10b, severe flow impacts, separations and wakes were induced by the blunt leading edge and thickness of the guide vanes, and the vorticities greatly increased in the annular convergent channel, leading to a higher entropy production. This implies that these wake flows had significantly enhanced the aerodynamic loss downstream of the guide vanes, especially on the side close to the entrance, and the uniformity of the flow parameters at the exit of the chamber was also greatly affected.

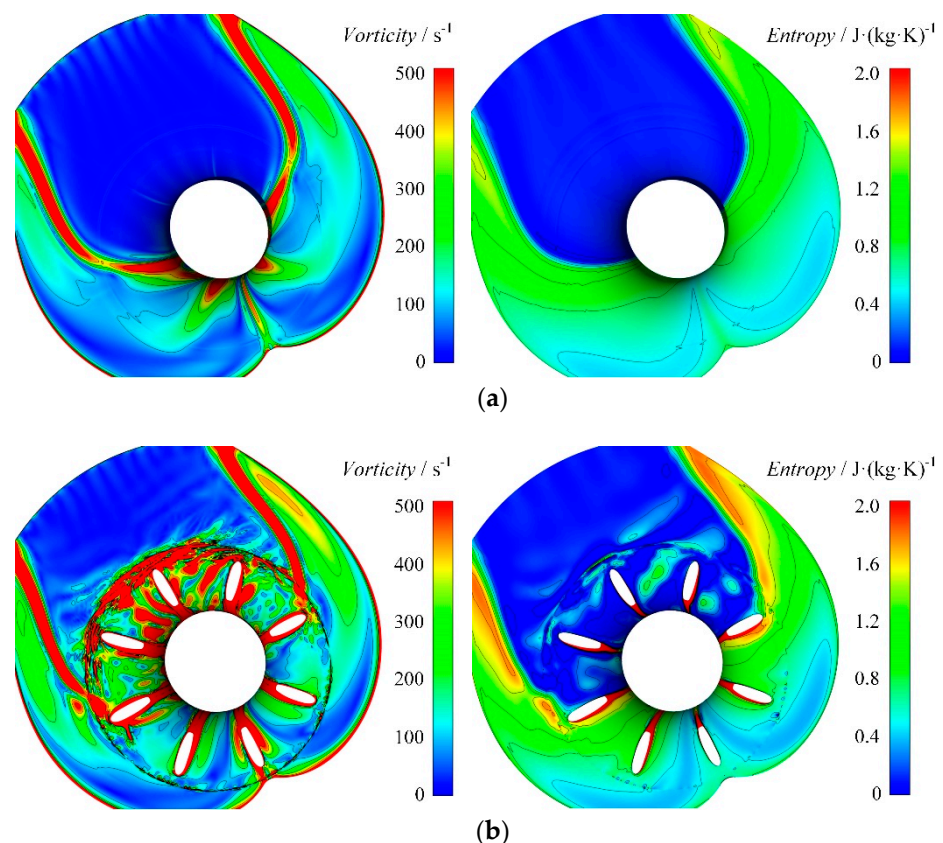


**Figure 10.** Flow conditions inside the spiral and annular convergence channels (a) without guide vanes and (b) with guide vanes.

In summation, in the scheme without guide vanes, the performance of the radial inlet chamber was mainly influenced by the sudden expansion and tangential flows in the spiral channel, as well as the flow separation at the 90° turning in the annular convergent channel. On the other hand, using the guide vanes would introduce additional flow impacts, separations and wakes, which further increased the flow loss in the radial inlet chamber.

#### 4. Performance Improvement and Downstream Effects

According to the flow analysis, the flow loss and unevenness of the radial inlet chamber were mainly generated in the spiral channel and annular convergent channel.

Therefore, the major geometric parameters of the relevant structures were selected and optimized in this section, including the radius  $r_c$  and width  $b_e$  of the spiral channel, the intersecting width  $w_e$  of the intake and spiral channels and the inlet width  $b_I$  of the annular convergent channel. Besides that, the structure of the intake channel was modified accordingly to make the flow passage from the entrance to the spiral channel smoothly connected. The purpose of the improvement in design was to reduce the flow loss, improve the internal flow conditions and achieve better performance from the radial inlet chamber by rearranging the flow area and the local flow rate at the key sections. The detailed geometric parameters of the improved geometry are listed in Table 4.

**Table 4.** Geometric parameters of the improved radial inlet chamber.

Item	Size
Inlet diameter of intake channel $D_{in}$	460 mm
Intersecting width of intake and spiral channels $w_e$	996 mm
Width of spiral channel $b_e$	330 mm
Radius of spiral channel $r_c$	576 mm
Inlet width of annular convergent channel $b_I$	220 mm
Inlet diameter of annular convergent channel $D_I$	440 mm

#### 4.1. Performance of the Radial Inlet Chamber

Figure 11 shows a comparison of the flow conditions in the original and improved radial inlet chambers under the design conditions. It can be clearly seen that as the geometric parameters  $r_c$ ,  $b_e$  and  $w_e$  increased, entropy production inside the entire inlet chamber was significantly reduced. Owing to the modifications on the intersection of the intake and spiral channels, the sudden expansion vortices were effectively suppressed at the inlet of the spiral channel, the size and strength of which were significantly reduced together with their influence on the downstream flow. In addition, on the other side of the spiral channel away from the intake, the bottom vortices generated by the improved inlet chamber were also weakened with a lower entropy. Therefore, the flow condition inside the optimized radial inlet chamber was improved, and the flow loss was significantly reduced.

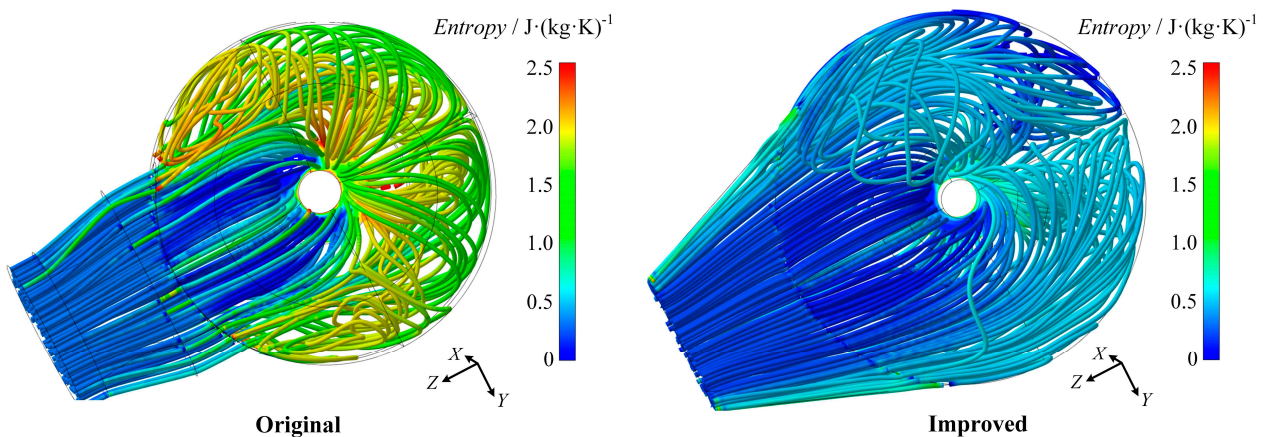


**Figure 11.** 3D flow conditions in the original and improved radial inlet chambers.

Detailed distributions of the Mach numbers and entropy at the exit of the spiral channel in the original and improved radial inlet chambers are shown in Figure 12. Compared with the flow pattern in the original one, the average flow speed in the improved structure greatly decreased, and the circumferential flow uniformity of this section increased. Meanwhile, entropy production in the improved spiral channel was much smaller, especially on the right side of this section. This indicates that the modification of the inlet chamber had significantly reduced the flow loss in the spiral channel—especially at the bottom of the

radial inlet chamber away from the intake—and improved the performance of the inlet chamber accordingly. The performance parameters of the original and improved radial inlet chambers have been compared in Table 5.

**Table 5.** Performance comparison of the original and improved radial inlet chambers.

Performance of the Inlet Chamber	Original	Improved
Efficiency $\eta_{ic}$	89.83%	94.86%
Total pressure loss coefficient $\zeta_{ic}$	1.1681	0.4472

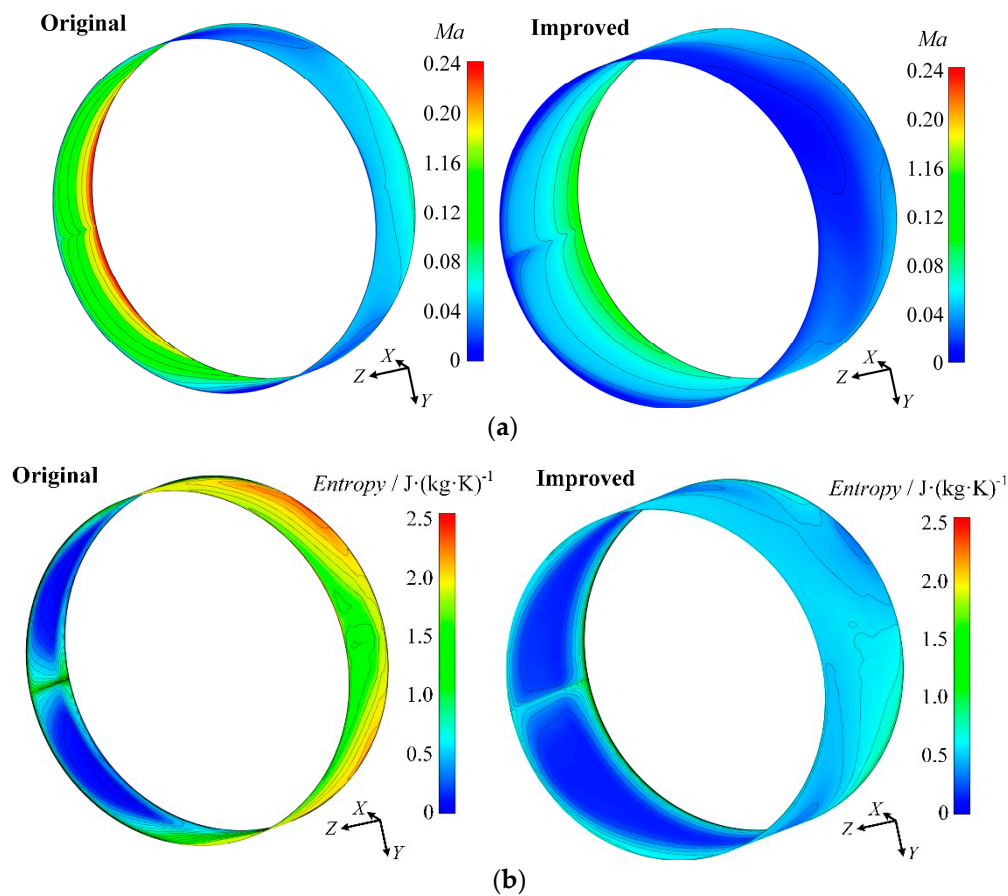


**Figure 12.** Flow conditions at the exit of the spiral channel. (a) Comparison of Mach numbers. (b) Comparison of entropy.

In addition, comparisons of the performance parameters under different operating conditions were also performed, as is shown in Figure 13. According to the performance curves of each radial inlet chamber, the total pressure loss coefficient decreased with the increase of the flow rate, and the efficiency of the inlet chamber increased accordingly. Furthermore, it can be clearly observed that the total pressure loss in the improved inlet chamber was significantly reduced under different operating conditions, and the corresponding efficiency was improved as well. By means of the improvement in this paper, the efficiency of the radial inlet chamber increased by 4.97% on average in the entire operating range, and the flow loss decreased by an average of more than 60%, achieving the purpose of improving the performance of the radial inlet chamber itself.



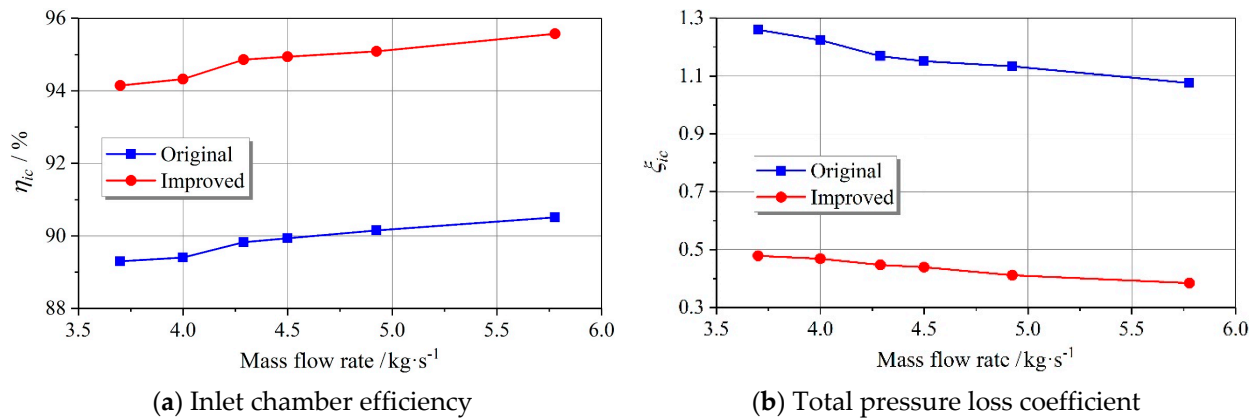


**Figure 13.** Performance comparison of the radial inlet chambers under different conditions.

#### 4.2. Effects on Downstream Components

In order to investigate the influence of structure modification on the downstream components, all the compressor stages with the improved and original inlet chambers were numerically analyzed and compared under the design conditions, as shown in Table 6. It was found that, although the efficiency of the inlet chamber itself increased by 5% after the modification, the performance of the entire compressor stage almost remained unchanged, even being slightly lower than that of the original stage. According to the comparison, the decrease in the impeller's efficiency was the main reason for the performance decrease of the stage with the improved inlet chamber. As is well known, impellers are the only working component in the compressors, and the impeller in the first stage generally operates with a medium or high-pressure ratio, which is crucial for the working capacity and performance of the whole machine. Therefore, besides the performance of the inlet chamber, the flow condition at the impeller inlet is also important for the performance of downstream components and the entire compressor.

**Table 6.** Performance comparison of the compressor stages with different inlet chambers.

Performance Parameter	Original	Improved
Stage efficiency $\eta_{in-out}$	80.38%	79.79%
Impeller efficiency $\eta_{0-2}$	95.27%	93.36%
Total pressure ratio $\epsilon_{in-out}$	1.2578	1.2561

Figure 14 shows the distributions of the major flow parameters at the impeller inlet, which is also the exit of the inlet chamber, including the total pressure, velocity magnitude and the tangential component of the velocity. It was found that, according to the improvement in the present study, not only the performance of the radial inlet chamber but also the uniformity of the flow condition at the impeller inlet was improved. In the original structure, a high pressure and high speed appeared in the region close to the intake channel, while a low total pressure with low speed occurred on the side away from the intake. In the results of the improved structure, high total pressures were evenly distributed at the impeller inlet, the unevenness of the velocity distribution almost disappeared in the circumferential direction, and the regions with greater tangential velocities were also stretched and weakened in this section. This indicates that part of the airflow which directly turned 90° to the annular convergent channel in the original structure was turned to the other side along the tangential direction of the spiral channel, realizing the redistribution of the flow rate inside the radial inlet chamber.



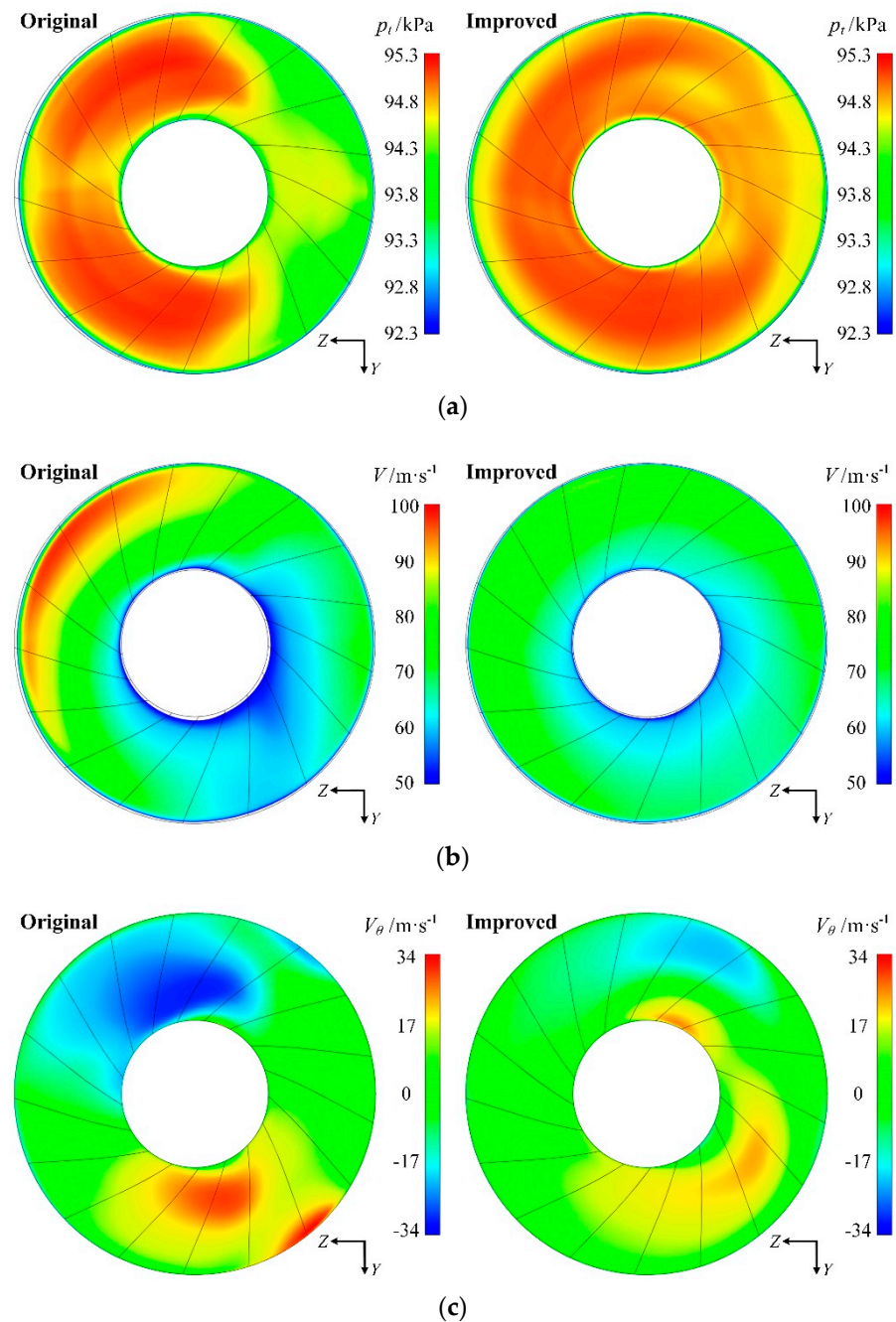


**Figure 14.** Flow contours at the impeller inlet. (a) Comparison of total pressures. (b) Comparison of velocity magnitudes. (c) Comparison of tangential velocities.

Generally, it was considered that an important reason for the performance decrease of the compressor stage with the radial inlet chamber was the non-uniformity of the flow distributions, since it was deviated from the ideal design condition of the impeller, which required an axial and uniform incoming flow. Although the structure modification in the present study improved the performance of the radial inlet chamber and increased the flow uniformity at the impeller inlet, the impeller efficiency was not improved. According to the flow distributions in Figure 14, it can be observed that the distributions of the total pressure and velocity magnitude in the improved scheme were closer to the axial inlet condition, and the distribution of the tangential velocity at the impeller inlet might be an essential factor for the whole compressor's efficiency. The values of the positive and negative tangential velocities at the exit of the original inlet chamber were greater, but

the circumferential range influenced by the positive tangential velocity was relatively concentrated, accounting for around 25% of the area. However, although the absolute values of the tangential velocities were reduced by more than 50% in the improved scheme, the area influenced by the positive tangential velocity accounted for over 60% of the area. This implies that more flow passages of the impeller were affected by the positive tangential velocities. When the tangential component of the velocity vector was consistent with the rotation direction of impeller (i.e.,  $V_\theta > 0$ ), flow separations were prone to occur on the pressure side of the blades, leading to a decrease in the working capacity of the impeller. The most probable reason for the increased circumferential range influenced by the positive tangential velocities is that the reduction of sudden expansions at the inlet of the spiral channel resulted in an increase of the tangential flow in the improved structure. Besides that, the airflow with a decreased velocity was more likely to be affected by the rotation of the downstream impeller, which further promoted the generation of positive tangential velocities. Therefore, it can be concluded that, for the improvement of a compressor stage with a radial inlet chamber, not only the performance of inlet chamber itself but also the uniformity of the flow condition at the impeller inlet should be considered, especially the positive tangential velocity, which is essential for the impeller's efficiency.

## 5. Conclusions

In this paper, the flow conditions inside the radial inlet chamber of an industrial centrifugal compressor stage were numerically investigated and improved by a new design. The purpose of the improved design is to reduce the flow loss and entropy production, improve the internal flow conditions and achieve better performance of the radial inlet chamber. The main measure was to rearrange the circumferential flow area and reduce the local flow rate at the key parts by modifying the major geometric parameters related to the spiral and annular convergent channels. In addition, increasing the intersection area and modifying the connection of the intake and spiral channels successfully suppressed the sudden expansion in the inlet chamber and its influence on the downstream flow. The results indicate that the improvement discussed in the present study can significantly reduce the total pressure loss and entropy production, increase the efficiency of the radial inlet chamber by an average of 4.97% over different operating conditions and enhance the uniformity of the flow distributions at the impeller inlet.

However, the improvement study also revealed that the increases in the performance and overall flow uniformity of the radial inlet chamber itself did not necessarily mean a performance improvement in the downstream components, and the distribution of the positive tangential velocity at the impeller inlet might be a more essential factor for the whole compressor's efficiency. For further improvement of the compressor stage with a radial inlet chamber, partial guide vanes with an optimized profile are recommended to control the positive tangential velocity at certain positions without greatly increasing the flow loss.

**Author Contributions:** Conceptualization, F.H., Y.M. and J.T.; methodology, F.H. and Z.W.; software, F.H.; validation, F.H., Y.M. and J.T.; formal analysis, F.H. and Z.W.; investigation, F.H.; writing—original draft preparation, F.H. and Z.W.; writing—review and editing, F.H. and Z.W.; project administration, W.L.; funding acquisition, F.H., Z.W. and W.L. All authors have read and agreed to the published version of the manuscript.

**Funding:** This research was funded by the National Natural Science Foundation of China (52006022), China Postdoctoral Science Foundation (2020M670726 and 2020M680928), National Key Research and Development Program of China (2018YFC0309003), 111 Project (B18009), Natural Science Foundation of Liaoning Province (2020-BS-067) and Fundamental Research Funds for the Central Universities (3132019368).

**Institutional Review Board Statement:** Not applicable.

**Informed Consent Statement:** Not applicable.

**Data Availability Statement:** Data sharing is not applicable to this article.

**Conflicts of Interest:** The authors declare no conflict of interest.

### Abbreviations

$D$	Diameter (m)
$Ma$	Mach number
$Q$	Volume flow rate ( $\text{m}^3 \cdot \text{s}^{-1}$ )
$T$	Temperature (K)
$p$	Pressure (Pa)
$U$	Peripheral speed/ $\text{m} \cdot \text{s}^{-1}$
$V$	Velocity ( $\text{m} \cdot \text{s}^{-1}$ )
$\varepsilon$	Total pressure ratio
$\eta$	Efficiency
$\kappa$	Isentropic exponent
$\xi$	Total pressure loss coefficient
$\rho$	Density ( $\text{kg} \cdot \text{m}^{-3}$ )
Subscript	
$in$	Stage inlet
$ic$	Inlet chamber
$out$	Stage outlet
$s$	Static condition
$t$	Total condition
$\theta$	Tangential component
0	Impeller inlet
2	Impeller outlet

### References

- Zhang, Q.; Huo, Q.; Zhang, L.; Song, L.; Yang, J. Effect of vaneless diffuser shape on performance of centrifugal compressor. *Appl. Sci.* **2020**, *10*, 1936. [\[CrossRef\]](#)
- Galindo, J.; Serrano, J.R.; Navarro, R.; García-Olivas, G. Numerical modeling of centrifugal compressors with heterogeneous incoming flow due to low pressure exhaust gas recirculation. In Proceedings of the ASME Turbo Expo 2020: Power for Land, Sea, and Air, Virtual, Online. 21–25 September 2020; V008T20A028.
- Cho, S.K.; Bae, S.J.; Jeong, Y.; Lee, J.; Lee, J.I. Direction for high-performance supercritical CO<sub>2</sub> centrifugal compressor design for dry cooled supercritical CO<sub>2</sub> Brayton cycle. *Appl. Sci.* **2019**, *9*, 4057. [\[CrossRef\]](#)
- Mojaddam, M.; Pullen, K.R. Optimization of a centrifugal compressor using the design of experiment technique. *Appl. Sci.* **2019**, *9*, 291. [\[CrossRef\]](#)
- Van den Braembussche, R. *Design and Analysis of Centrifugal Compressors*; John Wiley & Sons: West Sussex, UK, 2019; pp. 37–60.
- Shi, D.; Xie, Y. Aerodynamic optimization design of a 150 kW high performance supercritical carbon dioxide centrifugal compressor without a high speed requirement. *Appl. Sci.* **2020**, *10*, 2093. [\[CrossRef\]](#)
- Borovkov, A.; Voinov, I.; Galerkin, Y.; Kaminsky, R.; Drozdov, A.; Solovyeva, O.; Soldatova, K. Design, plant test and CFD calculation of a turbocharger for a low-speed engine. *Appl. Sci.* **2020**, *10*, 8344. [\[CrossRef\]](#)
- Liang, Q.; Zuo, Z.; Zhou, X.; Tang, H.; Chen, H. Design of a centrifugal compressor with low solidity vaned diffuser (LSVD) for large-scale compressed air energy storage (CAES). *J. Therm. Sci.* **2020**, *29*, 423–434. [\[CrossRef\]](#)
- Galindo, J.; Tiseira, A.; Navarro, R.; Tari, D.; Meano, C.M. Effect of the inlet geometry on performance, surge margin and noise emission of an automotive turbocharger compressor. *Appl. Therm. Eng.* **2017**, *110*, 875–882. [\[CrossRef\]](#)
- Eza, A. Flow Simulations with Relevance to a Centrifugal Compressor and the Effect of the Inlet Geometry. Master's Thesis, KTH Royal Institute of Technology, Stockholm, Sweden, 2015.
- Liu, M.; Tan, L.; Cao, S. A review of prewhirl regulation by inlet guide vanes for compressor and pump. *Proc. IMechE Part. A J. Power Energy* **2019**, *233*, 803–817. [\[CrossRef\]](#)
- Galindo, J.; Serrano, J.R.; Guardiola, C.; Cervelló, C. Surge limit definition in a specific test bench for the characterization of automotive turbochargers. *Exp. Therm. Fluid Sci.* **2006**, *30*, 449–462. [\[CrossRef\]](#)
- Galindo, J.; Serrano, J.R.; Margot, X.; Tiseira, A.; Schorn, N.; Kindl, H. Potential of flow pre-whirl at the compressor inlet of automotive engine turbochargers to enlarge surge margin and overcome packaging limitations. *Int. J. Heat Fluid Flow* **2007**, *28*, 374–387. [\[CrossRef\]](#)

14. MacManus, D.G.; Chiereghin, N.; Prieto, D.G.; Zachos, P. Complex aeroengine intake ducts and dynamic distortion. *AIAA J.* **2017**, *55*, 2395–2409. [[CrossRef](#)]
15. Yamada, K.; Furukawa, M.; Arai, H.; Ito, S. Effects of upstream bend on aerodynamic performance of a transonic centrifugal compressor. In Proceedings of the ASME Turbo Expo 2019: Turbomachinery Technical Conference and Exposition, Phoenix, AZ, USA, 17–21 June 2019; V02BT44A014.
16. Zhang, H.; Yang, C.; Yang, C.; Zhang, H.; Wang, L.; Chen, J. Inlet bent torsional pipe effect on the performance and stability of a centrifugal compressor with volute. *Aerosp. Sci. Technol.* **2019**, *93*, 105322. [[CrossRef](#)]
17. Zhou, S.; Lin, P.; Zhang, W.; Zhu, Z. Evolution characteristics of separated vortices and near-wall flow in a centrifugal impeller in an off-designed condition. *Appl. Sci.* **2020**, *10*, 8209. [[CrossRef](#)]
18. Zhu, W.; Ren, X.-D.; Li, X.-S.; Gu, C.-W. Analysis and improvement of a two-stage centrifugal compressor used in an MW-level gas turbine. *Appl. Sci.* **2018**, *8*, 1347. [[CrossRef](#)]
19. Flathers, M.B.; Bache, G.E.; Rainsberger, R. An experimental and computational investigation of flow in a radial inlet of an industrial pipeline centrifugal compressor. *J. Turbomach.* **1996**, *118*, 371–384. [[CrossRef](#)]
20. Koch, J.M.; Chow, P.N.; Hutchinson, B.R.; Elias, S.R. Experimental and computational study of a radial compressor inlet. In Proceedings of the ASME 1995 International Gas Turbine and Aeroengine Congress and Exposition, Houston, TX, USA, 5–8 June 1995; V001T01A014.
21. Michelassi, V.; Giachi, M. Experimental and numerical analysis of compressor inlet volutes. In Proceedings of the ASME 1997 International Gas Turbine and Aeroengine Congress and Exhibition, Orlando, FL, USA, 2–5 June 1997; V001T03A094.
22. Pazzi, S.; Michelassi, V. Analysis and design outlines of centrifugal compressor inlet volutes. In Proceedings of the ASME Turbo Expo 2000: Power for Land, Sea, and Air, Munich, Germany, 8–11 May 2000; V001T03A037.
23. Han, F.; Qi, D.; Tan, J.; Wang, L.; Mao, Y. Experimental and numerical investigation of the flow field in the radial inlet of a centrifugal compressor. In Proceedings of the ASME Turbo Expo 2012: Turbine Technical Conference and Exposition, Copenhagen, Denmark, 11–15 June 2012; pp. 831–845.
24. Han, F.; Mao, Y.; Tan, J.; Zhao, C.; Zhang, Y. Flow measurement and simulation of a radial inlet for centrifugal compressor. *Proc. IMechE Part A J. Power Energy* **2015**, *229*, 367–380. [[CrossRef](#)]
25. Kim, Y.; Koch, J. Design and numerical investigation of advanced radial inlet for a centrifugal compressor stage. In Proceedings of the ASME 2004 International Mechanical Engineering Congress and Exposition, Anaheim, CA, USA, 13–19 November 2004; pp. 127–139.
26. Saladino, A.J.; Bielecki, S.J. Streamlining of the radial inlet design process for centrifugal compressors. In Proceedings of the ASME 2002 International Mechanical Engineering Congress and Exposition, New Orleans, LA, USA, 17–22 November 2002; pp. 67–74.
27. Yagi, M.; Shibata, T.; Nishida, H.; Kobayashi, H.; Tanaka, M.; Sugimura, K. Optimizing a suction channel to improve performance of a centrifugal compressor stage. In Proceedings of the ASME Turbo Expo 2010: Power for Land, Sea, and Air, Glasgow, UK, 14–18 June 2010; pp. 2007–2017.
28. Kozhukhov, Y.V.; Yun, V.K.; Reshetnikova, L.V.; Prokopovich, M.V. Numerical investigation of different radial inlet forms for centrifugal compressor and influence of the deflectors number by means of computational fluid dynamics methods with computational model validation. *IOP Conf. Ser. Mater. Sci. Eng.* **2015**, *90*, 012047. [[CrossRef](#)]
29. Sezal, I.; Chen, N.; Aalburg, C.; Gadamsetty, R.K.V.; Erhard, W.; Del Greco, A.S.; Tapinassi, L.; Lang, M. Introduction of circumferentially nonuniform variable guide vanes in the inlet plenum of a centrifugal compressor for minimum losses and flow distortion. *J. Turbomach.* **2016**, *138*, 108–117. [[CrossRef](#)]
30. Tan, J.; Wang, X.; Qi, D.; Wang, R. The effects of radial inlet with splitters on the performance of variable inlet guide vanes in a centrifugal compressor stage. *Proc. IMechE Part C J. Mech. Eng. Sci.* **2011**, *225*, 2089–2105. [[CrossRef](#)]
31. Han, F.; Mao, Y.; Tan, J. Influences of flow loss and inlet distortions from radial inlets on the performances of centrifugal compressor stages. *J. Mech. Sci. Technol.* **2016**, *30*, 4591–4599. [[CrossRef](#)]
32. Galindo, J.; Dolz, V.; Tiseira, A.; Ponce-Mora, A. Numerical assessment of the dynamic behavior of a solar-driven jet-ejector refrigeration system equipped with an adjustable jet-ejector. *Int. J. Refrig.* **2021**, *121*, 168–182. [[CrossRef](#)]
33. Liu, X.; Wan, K.; Jin, D.; Gui, X. Development of a throughflow-based simulation tool for preliminary compressor design considering blade geometry in gas turbine engine. *Appl. Sci.* **2021**, *11*, 422. [[CrossRef](#)]
34. Wang, M.; Li, Y.; Yuan, J.; Osman, F.K. Influence of spanwise distribution of impeller exit circulation on optimization results of mixed flow pump. *Appl. Sci.* **2021**, *11*, 507. [[CrossRef](#)]
35. NUMECA International. *FINE™/Turbo. User Manual*; v12.1; NUMECA Int.: Brussels, Belgium, 2018.
36. Han, F.; Wang, Z.; Mao, Y.; Zhang, Y.; Tan, J. Large-scale flow measurements and analysis for radial inlets of industrial centrifugal compressors based on multi-hole probe system. *Int. J. Precis. Eng. Man.* **2019**, *20*, 79–92. [[CrossRef](#)]
37. Han, F.; Wang, Z.; Mao, Y.; Tan, J.; Li, W. Experimental and numerical studies on the influence of inlet guide vanes of centrifugal compressor on the flow field characteristics of inlet chamber. *Adv. Mech. Eng.* **2020**, *12*, 1687814020974909. [[CrossRef](#)]
38. Celik, I.B.; Ghia, U.; Roache, P.J.; Freitas, C.J. Procedure for estimation and reporting of uncertainty due to discretization in CFD applications. *J. Fluids Eng.* **2008**, *130*, 078001.
39. Yin, G.; Ong, M.C. On the wake flow behind a sphere in a pipe flow at low Reynolds numbers. *Phys. Fluids* **2020**, *32*, 103605. [[CrossRef](#)]

40. Han, X.; Kang, Y.; Sheng, J.; Hu, Y.; Zhao, W. Centrifugal pump impeller and volute shape optimization via combined NUMECA, genetic algorithm, and back propagation neural network. *Struct. Multidisciplinary Optim.* **2020**, *61*, 381–409. [[CrossRef](#)]
41. Putri, R.M.; Obhrai, C.; Jakobsen, J.B.; Ong, M.C. Numerical analysis of the effect of offshore turbulent wind inflow on the response of a spar wind turbine. *Energies* **2020**, *13*, 2506. [[CrossRef](#)]
42. Hildebrandt, A.; Ceyrowsky, T. One-dimensional and three-dimensional design strategies for pressure slope optimization of high-flow transonic centrifugal compressor impellers. *J. Turbomach.* **2019**, *141*, 051002. [[CrossRef](#)]